Self-Assembly of Alkylammonium Chains on Montmorillonite: Effect of Chain Length, Head Group Structure, and Cation Exchange Capacity

ARTICLE *in* CHEMISTRY OF MATERIALS · DECEMBER 2006

Impact Factor: 8.35 · DOI: 10.1021/cm062019s

4 AUTHORS, INCLUDING:

Hendrik Heinz
University of Akron
60 PUBLICATIONS **1,644** CITATIONS
SEE PROFILE

Ramanan Krishnamoorti
University of Houston
190 PUBLICATIONS **8,548** CITATIONS
SEE PROFILE

Barry L Farmer
Wright-Patterson Air Force Base
157 PUBLICATIONS **3,014** CITATIONS
SEE PROFILE

Self-Assembly of Alkylammonium Chains on Montmorillonite: Effect of Chain Length, Head Group Structure, and Cation Exchange Capacity

Hendrik Heinz,*[,†,‡] R. A. Vaia,[†] R. Krishnamoorti,[§] and B. L. Farmer[†]

Materials and Manufacturing Directorate, Air Force Research Laboratory, Wright Patterson AFB, Ohio 45433, Department of Mechanical and Materials Engineering, Wright State University, Dayton, Ohio 45435, and Department of Chemical Engineering, University of Houston, Houston, Texas 77204

Received August 26, 2006. Revised Manuscript Received September 30, 2006

The structure and dynamics of alkylammonium-modified montmorillonites with different cation exchange capacity (CEC), ammonium head groups, and chain length is investigated by molecular dynamics simulation for a large set of structures and compared to a wide array of experimental data. In the 44 systems, the relationship between computational (molecular dynamics) and experimental data (X-ray, IR, NMR, and DSC) was found to be very complementary. Much of the properties appear to be dictated through the inorganic−organic interface, which in addition to electrostatic interactions involves hydrogen bonds between primary ammonium head groups (NH_3^+−R) and oxygen on the silicate surface (O···H distance ∼150 pm) or flexibly attached quaternary ammonium head groups (NMe_3^+−R) of higher lateral mobility (O···H distance ∼290 pm). The gauche content is a function of the packing density of the head groups on the surface, the preferred orientation of the head groups, and the interlayer density of the alkyl chains. These effects cause up to 45% gauche conformations as compared to only 5% gauche conformations in chains with crystalline order. A low CEC leads to stepwise increases of the basal plane spacing with increasing chain length, corresponding to the subsequent formation of alkyl monolayers, bilayers, trilayers, etc., while a high CEC leads to a continuous increase in basal plane spacing with increasing chain length. The density of the organic interlayer space between two silicate layers shows minima for emerging new layers of alkyl chains and maxima for densely packed layers. These fluctuations decrease as the number of layers increases. On an isolated clay mineral surface, layer formation of the surfactants is also found and lateral 2D diffusion constants range from 5×10^{-6} cm^2/s to $<10^{-9}$ cm^2/s depending on the structure of the surfactant.

1. Introduction

Layered silicates[1] such as mica, montmorillonite, or pyrophyllite are abundant in soil and have many commercial applications, including rheology control agents,[2,3] substrates for nanopatterning,[4,5] and reinforcements in nanocomposites.[6,7] They are characterized by a layer-like shape, comparatively high mechanical stability at a thickness of 1 nm, and variations in color and shininess. Alkali metal ions are present naturally between the nanometer-thick layers, which can be exchanged with cationic surfactants such as octadecylammonium ions, to render the surface nonpolar. The hydrophilic nature of alkali-containing clay minerals and the lipophilic nature of organically modified clay minerals are exploited in drilling fluids, paints, cosmetics, greases, detergents, thin films, rubber, and plastics.[2−25] Surface modification can be achieved under mild conditions and

* To whom correspondence should be addressed. E-mail: hendrik.heinz@uakron.edu.
† Wright Patterson AFB.
‡ Wright State University.
§ University of Houston.

(1) We follow the nomenclature for "layer" and "sheet" as suggested by the International Association for the Study of Clays (AIPEA), i.e., the silicate "layer" of the clay minerals consists of tetrahedral and octahedral "sheets".

(2) Van Olphen, H. *An Introduction to Clay Colloidal Chemistry*; Wiley: New York, 1977.
(3) (a) Jones, T. R. *Clay Mineral.* **1983**, *18*, 399−410. (b) Kemnetz, S. J.; Still, A. L.; Cody, C. A.; Schwindt, R. *J. Coat. Technol.* **1989**, *61*, 47−55.
(4) Lagaly, G. In *Development of Ionic Polymers*; Wilson, A. D., Prosser, H. J., Eds.; Elsevier: New York, 1987; Vol. 2, pp 77−140.
(5) Wypych, G. *Handbook of Fillers*, 2nd ed.; ChemTec Publishing: Toronto, Canada, 1999.
(6) Ray, S. S.; Okamoto, M. *Prog. Polym. Sci.* **2003**, *28*, 1539−1641.
(7) *Functional Hybrid Materials*; Gómez-Romero, P., Sanchez, C., Eds.; Wiley-VCH: Weinheim, 2004.
(8) Lagaly, G.; Weiss, A. *Kolloid Z. Z. Polym.* **1970**, *237*, 364−368.
(9) Lagaly, G.; Weiss, A. *Kolloid Z. Z. Polym.* **1971**, *243*, 48−55.
(10) Lagaly, G. *Angew. Chem., Int. Ed.* **1976**, *15*, 575−586.
(11) Lagaly, G. *Clays Clay Miner.* **1982**, *30*, 215−222.
(12) Vaia, R. A.; Teukolsky, R. K.; Giannelis, E. P. *Chem. Mater.* **1994**, *6*, 1017−1022.
(13) Vaia, R. A.; Giannelis, E. P. *Macromolecules* **1997**, *30*, 7990−7999.
(14) Vaia, R. A.; Giannelis, E. P. *Macromolecules* **1997**, *30*, 8000−8009.
(15) Osman, M. A.; Seyfang, G.; Suter, U. W. *J. Phys. Chem. B* **2000**, *104*, 4433−4439.
(16) Manias, E.; Touny, A.; Wu, L.; Strawhecker, K.; Lu, B.; Chung, T. C. *Chem. Mater.* **2001**, *13*, 3516−3523.
(17) Ray, S. S.; Yamada, K.; Okamoto, M.; Ueda, K. *Nano Lett.* **2002**, *2*, 1093−1096.
(18) Osman, M. A.; Ernst, M.; Meier, B. H.; Suter, U. W. *J. Phys. Chem. B* **2002**, *106*, 653−662.
(19) Osman, M. A.; Ploetze, M.; Skrabal, P. *J. Phys. Chem. B* **2004**, *108*, 2580−2588.
(20) Zhu, J. X.; He, H. P.; Zhu, L. Z.; Wen, X. Y.; Deng, F. *J. Colloid Interface Sci.* **2005**, *286*, 239−244.
(21) He, H. P.; Ding, Z.; Zhu, J. X., Yuan, P.; Xi, Y. F.; Yang, D.; Frost, R. L. *Clays Clay Miner.* **2005**, *53*, 287−293.
(22) Osman, M. A.; Rupp, J. E. P.; Suter, U. W. *J. Mater. Chem.* **2005**, *15*, 1298−1304.

10.1021/cm062019s CCC: $37.00
Published on Web 12/13/2006

allows the introduction of a broad range of functionality in these hybrid systems. Addition of organically modified montmorillonites in polymer/layered silicate nanocomposites,[5−7,12−14,16,17,22] for example, can lead to higher moduli,[12−14] increased strength and heat resistance,[12−14] decreased gas permeability,[22] and flammability[16] as well as improved biodegradability.[17]

Thus, macroscopic properties in such systems can be engineered over a wide range and depend on the choice of the clay mineral and the surfactant. The understanding of interfacial interactions in these complex systems is currently limited and, ultimately, control over the nanoscale arrangement (morphology) of the silicate layers within a specific polymer, solvent, or other matrix remains an important challenge. The objective of this paper is to improve the necessary molecular-level understanding of self-assembly and dynamics for various surfactants on montmorillonite and similar surfaces.

Alkyl chains on montmorillonite surfaces were originally described by Lagaly and Dekany as stacked layers on the clay mineral surface containing all-anti conformations.[2,23] After Pechhold and co-workers established evidence of the occurrence of gauche conformations in layered alkyl chain aggregates,[26] Lagaly concluded that the formation of gauche conformations and kinks would also occur in alkyl chain aggregates on the surfaces of layered substrates.[10] The existence of conformational disorder in these systems was corroborated later by Vaia et al.[12] on the basis of IR measurements, and a multitude of techniques have since been employed to characterize organically modified montmorillonites, including X-ray diffraction, TEM, DSC, NEXAFS, NMR, IR, and dielectric spectroscopy.[8−10,12,14−23,25] The observation of phase transitions upon heating, variable chain conformations, and metastable phases motivated theory and simulation for explanations.[13,27−34] These properties generally depend on the cation exchange capacity (CEC) of the clay mineral, surfactant structure, and process history (annealing).[12,15,18,23,25,27−33] Coarse-grained[27−29] and atomistic models[30−34] provided understanding of the structure of the interlayer space between two silicate layers, chain conformations, and changes during phase transitions for selected systems. However, reliable simulations have been difficult due to coarse approximations in energy models, empirical distributions of charge defects, and simplifications of chemical detail in coarse-grain models.[34,35] Some of these limitations have been resolved in an advanced force field for layered silicates, which reproduces crystal structures, surface energies, and the distribution of charge defects in excellent agreement with experiment.[34]

Therefore, this work is a continuation of a series of papers[2−4,8−15,18−23,25,27−34] and attempts a coherent description of common alkylammonium chains on montmorillonite. The emphasis is on the structure and dynamics of the inorganic−organic interface, the influence of isomorphic substitution in the clay mineral, and components of the surfactant architecture (e.g., the cationic moiety and pendants) on the assembly of the surfactants between the silicate sheets, as well as on the establishment of a quantitative correlation between simulation and experiment. Control of these properties is critical for determining the compatibility with a variety of weakly bonded nanostructures, solvents, or polymer matrices. The conclusions serve as a guide to modify interfacial interactions, initiate polymerizations, and improve the strength of the interface between the aluminosilicate layers and adjacent moieties.

The outline of the paper is as follows. In section 2, computational procedures of the simulation and analysis are described. In section 3, molecular dynamics results are discussed for montmorillonite with a CEC of 91 and 145 mequiv/100 g (0.91 and 1.45 equiv/kg), NH_3 and NMe_3 head groups, and a series of alkyl chains from C_2 to C_{22}. In section 4, the computational results are compared to experimental data (XRD, IR, NMR, and DSC) to add fidelity to the interpretation of the molecular-level details and estimate the energetic barriers restricting mobility, as well as to verify the robustness of the simulation procedure. The paper concludes with a summary in section 5.

2. Computational Details

2.1. Force Field. We employ the polymer consistent force field (PCFF) with recent parameters for layered silicates[34] and the Discover program from Accelrys, Inc.[36] The semiempirical energy model for layered silicates takes surface energies accurately into account, and thus reproduces crystal structures, surface energies, and approximate vibrational frequencies of phyllosilicates in very good agreement with experiment.[34] Moreover, the PCFF (or COMPASS) parameters allow the quantitative reproduction of

(23) Lagaly, G.; Dekany, I. *Adv. Colloid Interface Sci.* **2005**, *114*, 189−204.
(24) Umemura, Y.; Shinohara, E. *Langmuir* **2005**, *21*, 4520−4525.
(25) Jacobs, J. D.; Koerner, H.; Heinz, H.; Farmer, B. L.; Mirau, P.; Garrett, P. H.; Vaia, R. A. *J. Phys. Chem. B*, in press.
(26) (a) Pechhold, W.; Blasenbrey, S. *Kolloid Z. Z. Polym.* **1967**, *216*, 235−244. (b) Pechhold, W.; Blasenbrey, S. *Kolloid Z. Z. Polym.* **1970**, *241*, 955−976. (c) Pechhold, W.; Liska, E.; Grossmann, H. P.; Hagele, P. C. *Pure Appl. Chem.* **1976**, *46*, 127−134.
(27) Haas, F. M.; Hilfer, R.; Binder, K. *J. Chem. Phys.* **1995**, *102*, 2960−2969.
(28) Hackett, E.; Manias, E.; Giannelis, E. P. *J. Chem. Phys.* **1998**, *108*, 7410−7415.
(29) Zeng, Q. H.; Yu, A. B.; Lu, G. Q.; Standish, R. K. *Chem. Mater.* **2003**, *15*, 4732−4738.
(30) Heinz, H.; Castelijns, H. J.; Suter, U. W. *J. Am. Chem. Soc.* **2003**, *125*, 9500−9510.
(31) Heinz, H.; Suter, U. W. *Angew. Chem., Int. Ed.* **2004**, *43*, 2239−2243.
(32) He, H. P.; Galy, J.; Gerard, J. F. *J. Phys. Chem. B* **2005**, *109*, 13301−13306.
(33) Gardebien, F.; Gaudel-Siri, A.; Bredas, J. L.; Lazzaroni, R. *J. Phys. Chem. B* **2004**, *108*, 10678−10686.
(34) Heinz, H.; Koerner, H.; Anderson, K. L.; Vaia, R. A.; Farmer, B. L. *Chem. Mater.* **2005**, *17*, 5658−5669. For the interaction between layers of layered silicates as a function of distance, see: Heinz, H.; Vaia, R.; Farmer, B. L. *J. Chem. Phys.* **2006**, *124*, 224713:1−9.
(35) (a) Sanders, M. J.; Leslie, M.; Catlow, C. R. A. *J. Chem. Soc., Chem. Commun.* **1984**, 1271−1273. (b) Beest, B. W. H.; Kramer, G. J.; Van Santen, R. A. *Phys. Rev. Lett.* **1990**, *64*, 1955−1958. (c) Skipper, N. T.; Refson, K.; McConnell, J. D. C. *J. Chem. Phys.* **1991**, *94*, 7434−7445. (d) Hill, J. R.; Sauer, J. *J. Phys. Chem.* **1995**, *99*, 9536−9550. (e) Fang, C. M.; Parker, S. C.; De With, G. *J. Am. Ceram. Soc.* **2000**, *83*, 2082−2084. (f) Greathouse, J. A.; Refson, K.; Sposito, G. *J. Am. Chem. Soc.* **2000**, *122*, 11459−11464. (g) Kuppa, V.; Manias, E. *Chem. Mater.* **2002**, *14*, 2171−2175. (h) Cygan, R. T.; Liang, J. J.; Kalinichev, A. G. *J. Phys. Chem. B* **2004**, *108*, 1255−1266. (i) Manevitch, O. L.; Rutledge, G. C. *J. Phys. Chem. B* **2004**, *108*, 1428−1435.
(36) *Cerius2* and *Discover* program. Discover User Guide, Version 96.0/4.0.0; Accelrys, Inc.: San Diego, CA, 2003.

densities, vaporization energies, and rotational energy barriers of hydrocarbons.[30]

2.2. Models. Montmorillonite models have been prepared according to the X-ray crystal structure.[34,37] The spatial distribution of Al → Mg charge defects in the octahedral sheet[1] is modeled in agreement with solid-state NMR data[31] and the assignment of charges at the defect sites has been previously discussed in detail.[38] Two common montmorillonite structures are considered, one with a cation exchange capacity (CEC) of 91 mequiv/100 g and another with a CEC of 145 mequiv/100 g. The chemical composition of the corresponding montmorillonite models is $Na_{0.333}[Si_4O_8][Al_{1.667}Mg_{0.333}O_2(OH)_2]$ and $Na_{0.533}[Si_4O_8][Al_{1.467}Mg_{0.533}O_2(OH)_2]$, respectively. The models closely resemble natural montmorillonite from Southern Clay Products and Nanocor, respectively. An uncertainty in CEC ±5% and additional isomorphous substitution, e.g., Al^{3+} → Fe^{3+},[37] can be found in the corresponding natural minerals.

Models of alkyl ammonium ions of the type $N(CH_3)_3^+-C_nH_{2n+1}$ and $NH_3^+-C_nH_{2n+1}$ with chain lengths $n = 2, 4, 6, ..., 22$ were prepared using the Cerius[2] graphical interface.[36] For $N(CH_3)_3$ head groups, the assigned partial charges are −0.10 for N and +0.275 distributed over each CH_3 group and the CH_2 group. For NH_3 head groups, the assigned partial charges are −0.50 for N, +0.4 for each H, and +0.3 distributed over the alpha CH_2 group.[34,38]

All systems are contained in a cubic box of 2.596 × 2.705 × 10 nm^3 size, based on a 5 × 3 × 1 unit cell of montmorillonite. Periodic boundary conditions are effective in the *x* and *y* directions while the systems remain open in the *z* direction to allow free equilibration of the gallery spacing.[39] Simulations with larger box size have shown that these dimensions suffice to keep finite size effects in the analysis very small.

2.3. Simulation. To ensure equilibration, the alkylammonium-montmorillonite structures were generated in two-step processes. First, a single montmorillonite layer surrounded by alkylammonium was constructed from an isolated montmorillonite layer and models of the alkylammonium ions. Alkali metal ions in equilibrium positions on the surface were quantitatively substituted with alkylammonium ions such that the ammonium head groups are positioned at the same location as previous alkali ions. Several structures with different orientation distribution of the alkyl chains were built for each system, subjected to a short energy minimization (200 steps conjugate gradient method), and subsequent NVT dynamics (600−2000 ps, in proportion to chain length). The equilibration of different start structures for a given alkylammonium surface density converged to very similar end structures. The structure of lowest energy was further equilibrated between 600 and 2000 ps, in proportion to chain length.

Next, two snapshots of equilibrated, single-layer alkylammonium montmorillonite were combined by uniformly offsetting coordinates within the simulation cell and subsequently decreasing the separation distance until alkyl chains were within a several hundred picometer distance. The duplicate assemblies were subjected to further molecular dynamics simulation (NVT ensemble) between 600 and 2000 ps, in proportion to chain length. Structures and energies were equilibrated after 200−600 ps, and snapshots were recorded during the second half of the trajectory to analyze structural and dynamic properties, using intervals between 1 and 3 ps in proportion to chain length. The calculation of meaningful ensemble averages is supported by the good correlation between independent data points for gallery spacings presented in Figures 1 and 2 below, in agreement with experimental data. A total of 44 different duplicate structures were independently prepared and equilibrated.

In all molecular dynamics simulations, the NVT ensemble, the Verlet integrator, a time step of 1 fs, a temperature of 298 K (maintained through velocity scaling), and summation of Coulomb and van der Waals interactions using the cell multipole method (fourth order, two layers of cells) were employed, using the Discover program from Accelrys, Inc.[36]

2.4. Analysis. Basal plane spacings (nm) have been computed as the mean center to center distance between the planes formed by octahedral Al atoms in the upper and lower layer of the clay mineral in the duplicate structures, as an average over 300 independent snapshots.

Interlayer densities (kg/m^3) have been calculated as the quotient of the mass of alkylammonium ions between the silicate layers and the associated interlayer volume. The interlayer volume is calculated according to $V_i = A_i h_i$, where A_i is the cross-sectional area of the box and h_i the interlayer height. The latter is obtained from the basal plane spacing by subtracting the constant value 0.919 nm, which corresponds to the mean gallery height of aluminosilicate layers without charge defects and interlayer material.[40]

The fraction of gauche conformations of the alkyl chains along the $N-C_n$ backbone has been calculated from the total number of $(n-2)$ torsional angles along the $N-C_n$ backbone. The calculation is performed separately for alkylammonium ions confined between the two montmorillonite layers and for alkylammonium ions on the surface of the layers to examine the effect of confinement. Averaging in the conformational analysis is performed over all alkylammonium ions in 300 snapshots, corresponding to a total of 10^4 to 10^5 torsion angles for each data point.

Diffusion coefficients *D* for alkylammonium ions on the montmorillonite surface (cm^2/s) have been calculated from the mean squared displacement of the head group nitrogen atoms $\langle r^2(t)\rangle$ over the entire trajectory time *t* in equilibrium, applying the Einstein relation $\langle r^2(t)\rangle = 2dDt$ for two-dimensional diffusion ($d = 2$).[41]

3. Simulation Results

In this section, the structure and dynamics of alkylammonium ions on montmorillonite will be described as seen in the simulation, including the structure of the inorganic−organic interface, basal plane spacings and annealing, the interlayer density, conformations of the alkyl chains on the inside (gallery) and on the outside of the silicate layers, and diffusion on the surfaces. The outside surface of the clay mineral is especially important because it builds the interface when dispersed in polymer media or solvents. Cation exchange capacities of 91 and 145 mequiv/100 g, $R-NH_3^+$ and $R-N(CH_3)_3^+$ head groups, and surfactant chain lengths ranging from C_2 to C_{22} are considered. As a visual guide in

(37) (a) Rothbauer, R. *Neues Jahrb. Mineral. Monatsh.* **1971**, 143−154. (b) Brown, G. *The X-ray Identification and Crystal Structures of Clay Minerals*; Mineralogical Society: London, 1961. (c) *Reviews in Mineralogy*; Bailey, S. W., ed.; Mineralogical Society of America: Chelsea, MI, 1988; Vol. 19. See also http://www.webmineral.com. (d) Lee, J. H.; Guggenheim, S. *Am. Mineral.* **1981**, *66*, 350−357. (e) Tsipurski, S. I.; Drits, V. A. *Clay Miner.* **1984**, *19*, 177−193. Mg positions not correct.

(38) Heinz, H.; Suter, U. W. *J. Phys. Chem. B* **2004**, *108*, 18341−18352.

(39) For a system of two layers with periodicity in the *xy* plane, an open box (equivalent to vacuum) in *z* direction is suitable to reduce periodicity to two dimensions. The associated decrease in vertical pressure (p_{zz}) is small compared to usual pressures in a NPT simulation (stretching of the system in *z* direction amounts to 2−3%). See: Heinz, H.; Paul, W.; Binder, K.; Suter, U. W. *J. Chem. Phys.* **2004**, *120*, 3847−3854.

(40) The value 0.919 nm corresponds to the basal plane spacing in pyrophyllite. Pyrophyllite is isomorphous (identical framework of covalent bonds) to montmorillonite when charge defects and associated interlayer material are absent (see ref 37d).

(41) Frenkel, D.; Smit, B. *Understanding Molecular Simulation*, ed. 2; Academic Press: San Diego, 2002.

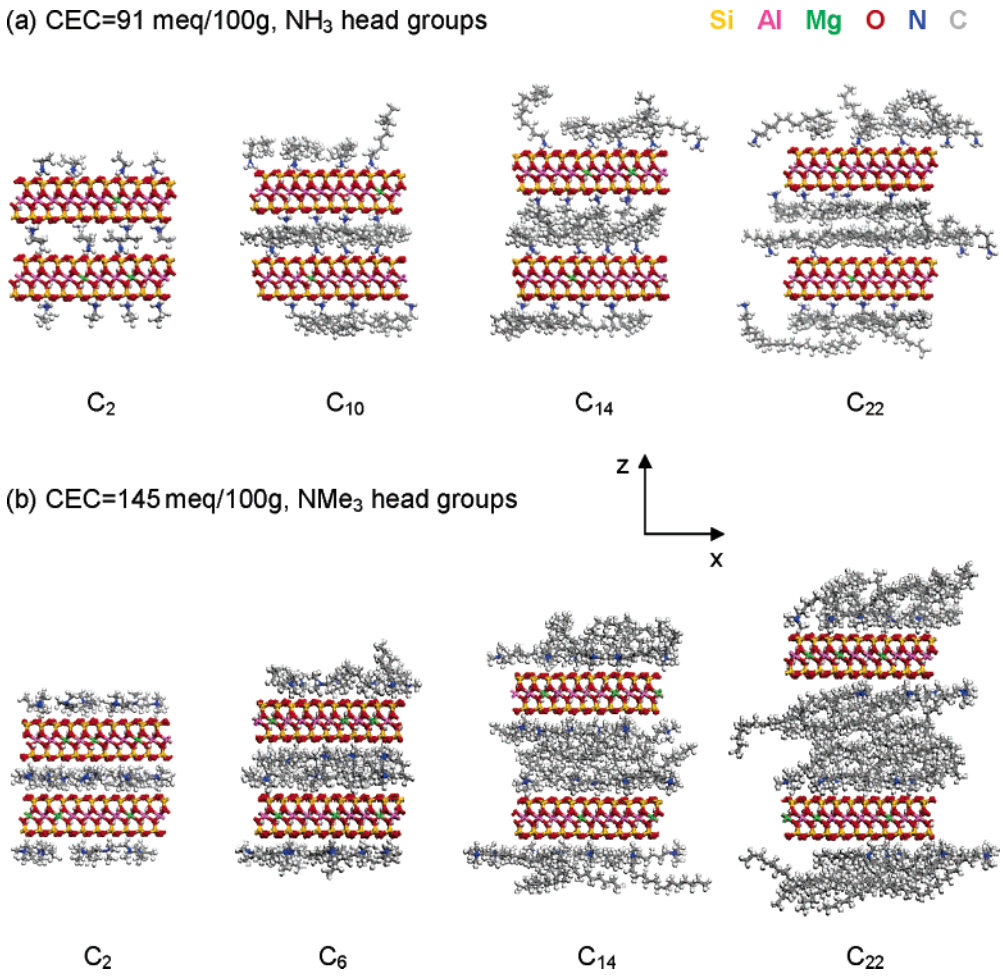

Figure 1. Representative MD snapshots of alkylammonium montmorillonites, viewed along the *y* direction. (a) CEC = 91 mequiv/100 g and $NH_3^+-C_n$ chains. The difference between partially formed layers (C_2, C_{14}) and completely formed layers (C_{10}, C_{22}) can be seen. (b) CEC = 145 mequiv/100 g and $NMe_3^+-C_n$ chains. The successive formation of layers with decreasing order can be seen.

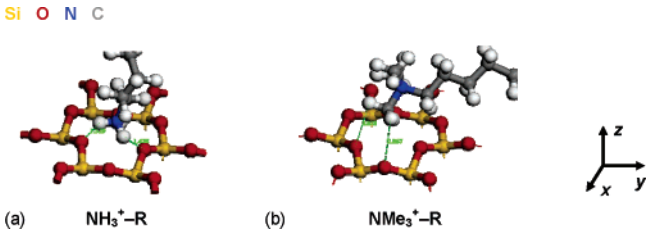

Figure 2. Organic−inorganic interface. (a) $R-NH_3^+$ head groups form hydrogen bonds to oxygen on the silicate surface. The average O···H distance is ∼150 pm and the mean N to O distance is 245 pm. (b) $R-N(CH_3)_3^+$ head groups do not form hydrogen bonds to the surface. The average O···H distance is almost twice as large, ∼290 pm, and the mean N to O distance is 390 pm. Qualitatively, this implies the mobility of the $R-NMe_3^+$ on the surface should be higher than that of $R-NH_3^+$.

the analysis, representative snapshots of the systems are displayed in Figure 1 and the structure of the inorganic−organic interface is shown in Figure 2.

3.1. Effect of the Head Group. As illustrated in Figure 2, the cationic head groups are positioned preferentially in cavities of (Si,O) 6-rings on the montmorillonite surface and ionically bonded to negatively charged Al → Mg defects in the octahedral sheet of the silicate layer. The functionality of the head group, however, affects the geometry and strength of the inorganic−organic interface and thus should impact the structure and dynamics of the surfactants on the surface of the clay mineral.

In addition to electrostatic bonding, the $R-NH_3^+$ head groups form N−H···O−Si hydrogen bonds to oxygen in the silicate surface with an average O···H distance of 150 pm (Figure 2a).[34,43] The formation of hydrogen bonds in this way was first described by Lagaly and Weiss for primary ammonium chains on mica,[8] and the hydrogen bond length is in the usual range of 130−200 pm.[44,45] Each of the three H atoms can approach an oxygen atom in the superficial cavity so that the N-terminal part of the surfactant shows a preference for an upright orientation relative to the surface (Figures 1a and 2a). The energetic gain from H-bonding is typically 1−4 kcal/mol per H bond[44,46] so that three possible hydrogen bonds per $R-NH_3^+$ head group suffice to offset increased conformational energy associated with changes in torsion angles from anti to gauche in the attached alkyl chain, which requires approximately ∼0.7 kcal/mol per gauche

(42) *CRC Handbook of Chemistry and Physics*, 84th ed.; Lide, D. R., Ed.; CRC Press: Boca Raton, FL, 2003.
(43) Geometry optimization of the silicate−primary ammonium interface at quantum-mechanical level using either Gaussian-type orbitals or plane waves supports the existence of N−H···O−Si hydrogen bonds with a bond length of approximately 160 pm.
(44) Jeffrey, G. A. *An Introduction to Hydrogen Bonding*; Oxford University Press: New York, 1997.
(45) Harris, T. K.; Mildvan, A. S. *Proteins* **1999**, *35*, 275−282.
(46) Sheu, S. Y.; Yang, D. Y.; Selzle, H. L.; Schlag, E. W. *Proc. Natl. Acad. Sci. U.S.A.* **2003**, *100*, 12683−12687.

conformation.[47] The percentage of gauche torsions is thus higher in short chains with $R-NH_3^+$ head groups relative to short chains with $R-NMe_3^+$ head groups (see sections 3.4 and 3.5 and Figures 3c, 4c, and 5). The effect decreases for longer chains because the relative interlayer volume away from the aluminosilicate surface increases and optimum van der Waals interactions between the alkyl chains become dominant.

In contrast, $R-N(CH_3)_3^+$ head groups cannot form hydrogen bonds to the surface and the average O···H distance amounts to 290 pm (Figure 2b). In addition, the bulky methyl groups act as a spacer to keep the cationic N center farther away from the montmorillonite surface (Figure 1b). This leads to a flexible orientation of the $R-NMe_3^+$ head group on the surface and greater lateral mobility, including rearrangements across cavities[30] and a higher rate of diffusion (see section 3.6).

When $R-NMe_3^+$ surfactants are compared with $R-NH_3^+$ surfactants, plots of gallery height and changes in interlayer density (see sections 3.2 and 3.3, Figures 3 and 4) are shifted on average by $\Delta n \approx 2$ carbon units rather than by $\Delta n \approx 3$ carbon units. Therefore, the three extra methylene units tethered into the $R-NMe_3^+$ head group exhibit an effect similar to only two additional methylene units in the open backbone. The "third" CH_2 group in quaternary alkylammonium chains leads to a higher interlayer density relative to primary alkylammonium chains (Figures 3b and 4b) when the curves of interlayer density are corrected for the offset $\Delta n \approx 2$. As would be expected due to the decreasing contribution of the head group to overall surfactant volume, the difference in interlayer density due to this effect decreases for longer chains.

3.2. Basal Plane Spacing. At a low cation exchange capacity (CEC = 91 mequiv/100 g), a stepwise increase in basal plane spacing with increasing chain length is observed (Figure 3a). Beginning essentially with the head groups between the two mineral surfaces themselves, an alkyl monolayer is gradually formed until complete at a chain length of C_8 (NMe_3 head group) or C_{10} (NH_3 head group). Then follows a transition to an alkyl bilayer, which is increasingly filled with interlayer material until complete at a chain length of C_{20} (NMe_3 head group) or C_{22} (NH_3 head group). The process of "filling" the layers is illustrated in Figure 1a for the series with NH_3 head groups. This verifies in a quantitative manner what has been observed and concluded in the past (see section 4.1).[9,12,14,19,22,23] The well-defined and extensive series here captures even more insight into the fidelity and nature of the steps.

At a high cation exchange capacity (CEC = 145 mequiv/100 g), only a weak steplike pattern can be discerned and alkylammonium montmorillonites exhibit a continuous increase in gallery spacing with increasing chain length (Figure 4a). A densely packed alkyl monolayer is formed at a chain length of C_4 (NMe_3 head group) or C_6 (NH_3 head group), a densely packed bilayer at C_{10} (NMe_3 head group) or C_{12} (NH_3 head group), a densely packed trilayer at C_{16} (NMe_3 head group) or C_{18} (NH_3 head group), and the equivalent of a densely packed 4-layer at C_{22} (NMe_3 head group). This process is illustrated in Figure 1b for the series with NMe_3 head groups. In principle, we observe here the same effect of successive layer "filling" as at a lower CEC; however, the higher density of head groups per surface area makes the formation of sharply defined layers more difficult. Thus, the system is closer to a densely packed, self-assembled monolayer with a specific tilt angle relative to the surface normal.

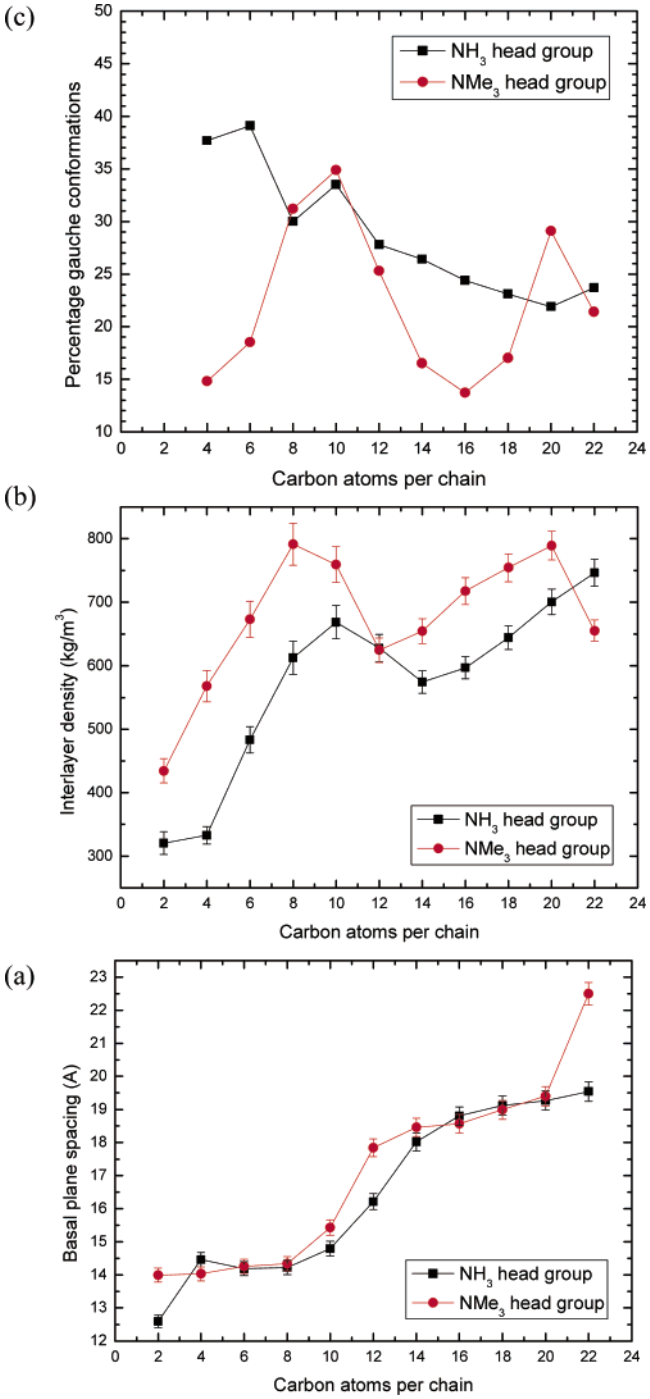

Figure 3. (a) Computed basal plane spacing, (b) interlayer density, and (c) average conformation of the alkyl chains between the silicate layers for alkylammonium-modified montmorillonite with CEC = 91 mequiv/100 g. The series $NH_3^+-C_nH_{2n+1}$ and $N(CH_3)_3^+-C_nH_{2n+1}$ with n = 2, 4, ..., 22 are shown.

(47) Herrebout, W. A.; van der Veken, B. J.; Wang, A.; Durig, J. R. *J. Phys. Chem.* **1995**, *99*, 578−585.

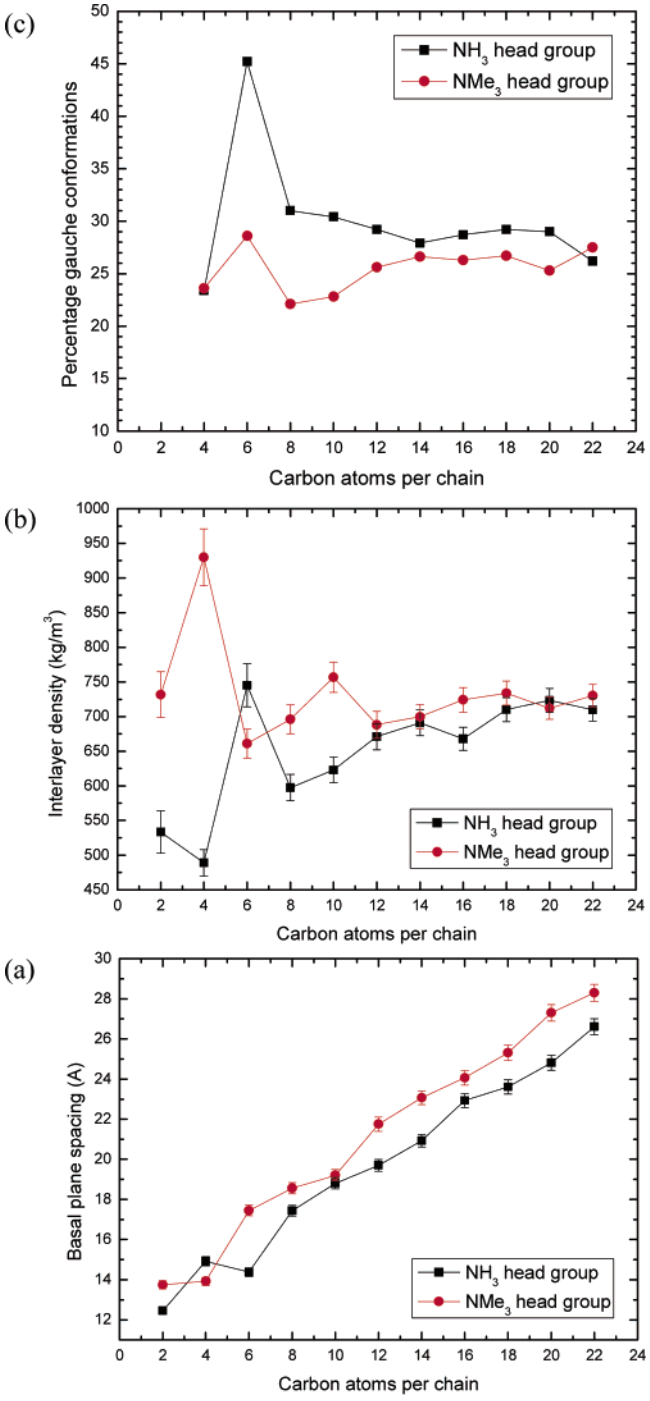

Figure 4. (a) Computed basal plane spacing, (b) interlayer density, and (c) average conformation of the alkyl chains between the silicate layers for alkylammonium-modified montmorillonite with CEC = 145 mequiv/100 g. The series $NH_3^+-C_nH_{2n+1}$ and $N(CH_3)_3^+-C_nH_{2n+1}$ with n = 2, 4, ..., 22 are shown.

3.3. Interlayer Density. The relatively constant gallery spacing at lower CEC for a range of alkyl chains with various sizes causes periodic fluctuations in interlayer density (Figure 3b). The interlayer density is minimal for a partially formed layer and maximal at an alkyl chain length yielding a "complete" layer. For example, after the first layer is densely packed, additional interlayer material (alkyl groups) must be accommodated by gallery expansion, which creates a partial second layer and an overall decrease in interlayer density. This partial new layer frustrates close packing of the hydrocarbons so that the interlayer density remains lower until filled with more backbone atoms to complete a densely packed second layer. At lower CEC, this "layering" effect is enhanced due to the lower surface density of surfactants and thus greater propensity for lateral (in-plane) conformations of the alkyl chain.

When the CEC is higher (Figure 4b), the formation of new layers is also accompanied by periodic fluctuations in interlayer density. However, due to the higher surface density of surfactants, the alkyl chains must adopt conformations that favor more of a perpendicular orientation to the aluminosilicate surface. Thus, the "layers" are less distinctly formed; the amplitude of fluctuations in interlayer density is smaller and decreases with the formation of increasingly homogeneous multilayered structures. The interlayer density converges for surfactants with both head groups to ~725 kg/m^3. This value is 8% less than the experimentally measured density 790 kg/m^3 of comparable crystalline *n*-alkanes (C_{20}, C_{22}).[42] The difference is in agreement with the liquid-like state of the hydrocarbon chains in the interlayer space between the two silicate layers (section 3.4) in comparison to a more densely packed crystal.

3.4. Conformation of the Alkyl Chains between the Silicate Layers. The conformation of the alkyl chains between the two silicate layers varies between 14% and 45% gauche as a function of CEC, head group structure, and chain length (Figures 3c and 4c). Therefore, the average fraction of gauche conformations at room temperature is found to be higher than that in a typical hydrocarbon crystal (~5% gauche in solid octadecylamine)[31,34] and may exceed typical values for a hydrocarbon liquid (~39% gauche, liquid octadecylamine)[34] in extreme cases.

At a low CEC (Figure 3c), the type of head group (primary vs quaternary) has a large influence on the conformer content. For primary ammonium, the percentage of gauche conformers generally decreases with increasing chain length. In contrast, for the quaternary ammonium, large fluctuation in gauche conformer content occurs at the alkyl chain lengths corresponding to complete layers. Surfactants with quaternary head groups have no orientation preference on the surface due to specific ammonium-aluminosilicate bonding, so as the alkyl length increases, there is considerable conformational freedom of the entire surfactant on the surface to adopt the lowest energy anti-conformers. As the density increases, however, confinement and volume-filling requirements of the densely packed interlayer space (C_8-C_{10}, C_{20}) greatly increase the gauche content (Figure 3c). After these constraints are released by the adoption of a larger gallery height and lower interlayer density, the alkyl chains can adopt the lower energy anti conformations. Surfactants with primary ammonium head groups, however, form favorable hydrogen bonds to the surface (Figure 2), which dictate the relative orientation of the α-methyl groups with respect to the surface. Thus, to accommodate the three hydrogen bonds, the alkyl chains must adopt a gauche conformation near the primary ammonium. Due to the small number of methyl units, this effect dominates the overall percentage of gauche torsions for shorter chains. The relative impact on the overall percentage of gauche torsions decreases with increased chain

length (Figure 3c). Moreover, an additional increase in gauche content with the onset of a complete layer (C_{10}, C_{22}) can still be observed.

At higher CEC (Figure 4c), the general features discussed above are also present. For primary ammonium, the percentage of gauche conformer decreases with increased chain length; for quaternary ammonium, fluctuations in percentage of gauche conformer correspond with step increases in the gallery height. However, the magnitude of these effects is substantially reduced. Overall, the percentage of gauche conformers, at least for mid- and long-chain alkyls, is relatively constant (22−28%), in contrast to changes from 15 to 35% at low CEC. The higher density of head groups per surface area enforces a preferential orientation of the surfactant with respect to the aluminosilicate layer, irrespective of the specific bonding between the ammonium head group and the aluminosilicate surface. Rather than simply tilting an all-anti chain conformation, volume packing considerations are addressed by accommodating a substantial degree of disorder, raising the gauche fraction above 20%. In agreement with the smaller fluctuations in interlayer density and weaker definition of alkyl layers, the overall fluctuation in chain conformations is less, e.g., the range for NMe_3^+-R is between 22 and 28% gauche (Figure 4c). Additionally, the percentage of gauche conformations for longer chains converges to an average 27% with both NH_3 and NMe_3 head groups, consistent with a transition from consecutively filled layers to a continuously increasing interlayer space between the two silicate layers for longer alkyl chains. At the smallest chain lengths, the percentage of gauche conformations is still higher for NH_3 head groups due to hydrogen bonds to the surface (Figure 2). The highest incidence of gauche conformations (45%) is seen for $H_3N^+-C_6H_{13}$ chains where the backbone is fitted into an alkyl monolayer in the presence of these hydrogen bonds (section 3.1).

In conclusion, the main factors controlling the degree of conformational disorder appear to be the following: (1) the density and distribution of charge defects in the mineral which determine the localization of the ammonium head groups[34] and introduce a minimum level of disorder in the backbones, (2) preferences in orientation of the head groups on the surface such as hydrogen bonds between the surface and $R-NH_3^+$ head groups, and (3) the degree of volume packing of the hydrocarbon chains as reflected by the interlayer density.

3.5. Conformation of the Alkyl Chains on the Outside of the Silicate Layers. Before going into detail, we remind the reader that we consider the interface of modified silicate layers to vacuum. It is essentially an interface to a non-interacting medium, and there would be additional effects if a solvent, a polymer, or an adsorbent vapor is present.

The average chain conformation on the outer surface of the silicate layers is shown in Figure 5. The absence of confinement leads to weaker fluctuations in average conformation. Nevertheless, the degree of conformational disorder on the outer surface can be understood by the same factors as for alkyl chains between the layers. The average fraction of gauche conformations for longer chains on the outer surface approaches 25% under ambient conditions, similar to the alkyl chains between the silicate surfaces. Additionally, a process of layering is seen with increasing chain length, although less defined than between the silicate layers (Figure 1). These observations are in agreement with experimental evidence for surface crystallinity in liquid *n*-alkanes above the freezing point.[48]

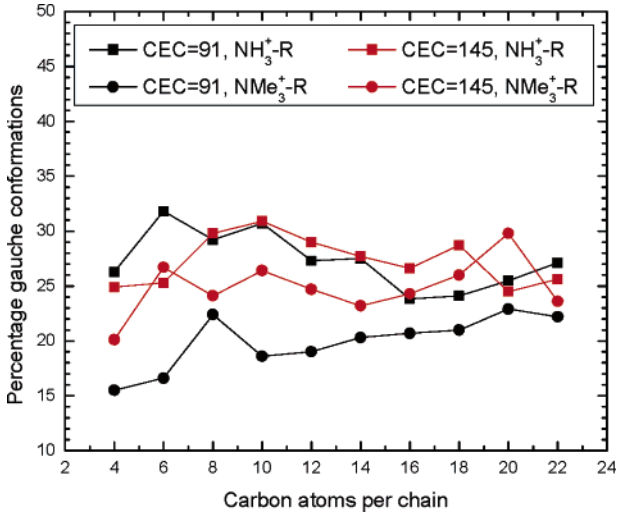

Figure 5. Average conformation of the alkyl chains on the outside of the surfactant-modified montmorillonite layers. The statistical uncertainty is less than ±0.5% gauche conformations.

At low CEC, NH_3 head groups cause a higher fraction of gauche conformations for shorter chains compared to NMe_3 head groups, resulting from the formation of favorable hydrogen bonds to the surface (Figure 2). Similar to the interlayer space between two silicate layers, the relative percentage of gauche conformers decreases as the total number of carbon atoms in the alkyl corona increases. A small increase in gauche conformations toward C_{20} for the quaternary ammonium ions (C_{22} for the primary ammonium ions) may be associated with the formation of a weakly defined monolayer through stronger chain−chain interactions (Figure 1a), even though confinement on the outer surfaces is absent.

At higher CEC, the higher density of head groups increases the conformational disorder of the quaternary ammonium surfactants (Figure 5). For the primary ammonium surfactants, however, a higher gauche fraction than at lower CEC is not seen because there may be more chain−chain dispersive interactions and less chain−surface interactions that lead to extra gauche conformations at lower CEC (Figure 1b). The formation of weakly defined monolayers and bilayers on the outer surfaces (Figure 1) is indicated for NMe_3 head groups by small increases in the gauche percentage toward C_8 and C_{20}. It must be kept in mind, though, that these differences amount to only 0.2−1.5 gauche torsions per chain (even though several 10^3 alkyl chains are included in the analysis).

3.6. Diffusion. Diffusion of surfactants on the montmorillonite surface can have two possible causes: hopping across the cavities due to Brownian motion or concentration

(48) Wu, X. Z.; Ocko, B. M.; Sirota, E. B.; Sinha, S. K.; Deutsch, M.; Cao, B. H.; Kim, M. W. *Science* **1993**, *261*, 1018−1021.

Table 1. Comparison of Experimental and Computed Basal Plane Spacings (nm)[a]

	expt[b] CEC = 90 Me_3NR^+	sim CEC = 91 Me_3NR^+	expt[c] CEC = 90 H_3NR^+	sim CEC = 91 H_3NR^+	expt[d,e] CEC = 150 H_3NR^+	sim CEC = 145 H_3NR^+
C_4	1.42 (2)	1.40 (2)	1.36 (3)	1.45 (2)		
C_6			1.36 (3)	1.42 (2)	1.50 (3)	1.44 (2)
C_8	1.42 (2)	1.43 (2)	1.36 (3)	1.42 (2)		
C_{10}			1.45 (3)	1.48 (3)	1.80 (3)	1.89 (3)
C_{12}	1.66 (9)	1.78 (3)	1.70 (3)	1.62 (3)	1.87 (3)	1.97 (3)
C_{14}	1.77 (10)	1.85 (3)	1.75 (3)	1.80 (3)	2.03 (3)	2.09 (3)
C_{16}	1.81 (10)	1.86 (3)	1.75 (3)	1.88 (3)	2.28 (3)	2.29 (3)
C_{18}	1.85 (3)	1.90 (3)	1.85 (2)	1.91 (3)	2.30 (3)	2.36 (3)
std dev to expt		0.07		0.08		0.08

[a] Standard deviations of the last digit are given in parentheses. [b] References 19 (C_4, C_8), 22 (C_{18}), and 50. [c] Reference 9, further supported by ref 23. [d] Reference 12. Reference 14 corroborates the value for C_{18}. [e] For CEC = 150, NMe_3 head groups, a reference value was found only for C_{18}: 2.52 (3) nm (ref 14) vs 2.53 (3) nm in the simulation.

gradients of defect sites (only possible if ion exchange with surfactants would be incomplete). Here we observe self-diffusion by Brownian motion only, i.e., the exchange rate between adjacent surfactants. Characteristic for the motion of the surfactants is a correlation between a group of at least two surfactants that results from their desire to remain close to the charge defects.

The surfactants in the interlayer space between two silicate layers show virtually no lateral mobility in the simulation, independent of CEC, head group, and chain length. 2D diffusion constants at room temperature are $\leq 10^{-9}$ cm^2/s, related to close packing of the chains. Self-diffusion then involves conformational changes in the backbone and concerted movements of alkylammonium ions (Figure 1), which is associated with high-energy barriers. Qualitatively, we expect the lowest diffusion constants (and highest energy net barriers) for high CEC, H-bonded NH_3 head groups, and long alkyl chains.

As a result, significant diffusion can only be found on single surfaces, i.e., on the outside of the duplicate structures. The order of magnitude of the rate of diffusion is still sensitive to the CEC, head group chemistry, and chain length. (1) Surfactants with NH_3 head groups (both at low and at high CEC, any chain length) yield either no net movement on the surface or occasional jumps to a neighbor cavity at a time scale of 1 ns. (2) Alkyl chains with NMe_3 head groups exhibit more frequent hopping on the surface. However, at CEC = 145 mequiv/100 g for any chain length and at CEC = 91 mequiv/100 g for chains longer than C_6, 2D diffusion constants remain $<10^{-7}$ cm^2/s. (3) In contrast, notably rapid motion on the surface is seen for the smallest quaternary ammonium ions at low CEC. Computed 2D diffusion constants are 5.0×10^{-6} cm^2/s for Me_3NEt^+ and 1.5×10^{-6} cm^2/s for Me_3NBu^+ at CEC = 91 mequiv/100 g, which amounts to approximately 20% and 6% of the 3D self-diffusion constant of liquid water at room temperature (2.3×10^{-5} cm^2/s).

In conclusion, various degrees of mobility are possible and remarkably rapid motion on the surface occurs for short quaternary alkylammonium ions on single surfaces of low CEC.

4. Comparison with Experiment

In this section, experimental data from X-ray diffraction (XRD), TEM, IR, and NMR spectroscopy, and DSC[9,12,14,19−23,25,49,50] are compared to simulation results. Overall, the structure (XRD, TEM), chain conformations (IR, NMR), and thermal behavior of the organically modified montmorillonites on heating (DSC, IR, NMR) are very well reproduced in the simulation, which establishes confidence in the molecular-level interpretation introduced in the previous section.

4.1. Structure. The occurrence of stepwise increases in gallery spacing at approximately 1.4, 1.8, and 2.15 nm for an alkyl monolayer, bilayer, and trilayer at low CEC in the computational model (Figure 3a) is in quantitative agreement with experimental observations by Lagaly and co-workers.[9,23] The trend toward a continuous increase in gallery spacing at higher CEC (Figure 4a) agrees with results from Vaia et al.,[12] and the structure of representative snapshots (Figure 1) resembles closely the TEM micrographs recorded by Drummy et al.[49]

In detail, computed basal plane spacings are compared to experimental data from X-ray diffraction in Table 1.[9,12,14,19,22,23] The average deviation amounts to ±0.08 nm (±5%), which is within the computational and experimental errors. Computed gallery spacings tend to be overestimated by 2−3% relative to experiment, owed to the limited accuracy of the energy model and the open box in *z* direction.[39] Uncertainties in experimental gallery spacings are associated with a distribution of interlayer environments due to heterogeneities within the natural montmorillonite, uncertainty in CEC (±5 mequiv/100 g), and nonequilibrium structures in the interlayer space depending on the process history of the sample.[14] Besides, residual amounts of water may be present in the sample.

Though it may be difficult to explain the small deviations correctly, we find that in cases with uncertainty in CEC,[9,12,14,23,50] deviations in gallery height tend to be higher, particularly at the onset of steps in gallery spacings vs chain length (Figure 1a). When the CEC was accurately determined, e.g., at CEC = 90 mequiv/100 g for NMe_3 head groups with C_4, C_8, and C_{18},[19,22] simulation and experiment are in best agreement (Table 1). Simulation of thermal cycling of representative structures yields a compression in

(49) Drummy, L. F.; Koerner, H.; Farmer, K.; Tan, A.; Farmer, B. L.; Vaia, R. A. *J. Phys. Chem. B* **2005**, *109*, 17868−17878.

(50) X-ray diffraction for the determination of the montmorillonite gallery spacings was conducted on a Bruker AXS D8 Discover at the Cu Kα wavelength of 1.5418 Å.

Table 2. Basal Plane Spacings (nm) before and after Computer Simulation of Annealing for Montmorillonite with CEC = 91 mequiv/100 g and Me_3N^+-R Surfactants

	start (298 K)	heated (448 K)	annealed (298 K)
C_{12}	1.78 (3)	1.835 (30)	1.787 (14)
C_{14}	1.85 (3)	1.893 (30)	1.807 (17)
C_{16}	1.86 (3)	1.911 (27)	1.839 (14)
C_{18}	1.90 (3)	1.932 (35)	1.867 (14)

gallery height of 0 to 3% (Table 2), which is similar to experiment (up to 5% compression after several cycles). The molecular scale process leading to an increased interlayer density appears to be the relaxation of interchain and chain−surface interactions. Further quantitative exploration of these effects could be carried out by a thorough investigation of the energy landscape and its local energy minima;[51] however, it is not the subject of the present paper.

4.2. Chain Conformation. IR[12,15,18−20] and NMR[18−20] spectroscopy have been employed to monitor conformations of the alkyl chains as a function of CEC, head group chemistry, chain length, and temperature. In IR spectroscopy, an increase in energy (wavenumbers) of the symmetric and of the antisymmetric CH_2 ($\nu_{s,CH2}$ and $\nu_{a,CH2}$) stretching vibration by a few cm^{-1} indicates an increase in gauche conformations. The values of $\nu_{s,CH2}$ and $\nu_{a,CH2}$ typically change from 2848 to 2854 cm^{-1} and from 2917 to 2928 cm^{-1}, respectively, during a solid−liquid transition, with the absolute values depending somewhat on the system.[12,15,19,20] Similarly, ^{13}C NMR spectral shifts for backbone CH_2 groups indicate an all-anti conformation with a single peak at 33 ppm and the presence of gauche conformations with the combination of a weaker single peak at 33 ppm and a second peak at 30 ppm.[18,52] In contrast to IR spectroscopy, NMR is more quantitative, and the absolute values are reproducible in different systems.[18−20] Relaxation processes on larger time scales (ms and s) can also be studied.[52]

For organically modified montmorillonites with low CEC (72 and 58 mequiv/100 g), NMe_3 head groups, conformational disorder is observed in NMR spectroscopy for C_{16} and C_{18} chains (peaks at both 30 and 33 ppm).[19,20] Partial disorder is also indicated in IR spectroscopy (peaks at 2851 and 2920 cm^{-1}).[20] This is in support of a liquid-like state observed in the simulation (Figure 3c) and a gauche content lower than that in liquid octadecylamine under ambient conditions. Upon heating, CH_2 stretching vibrations retain their frequency[19] and no order−disorder transition is observed in DSC (see section 4.3),[19,25] consistent with simulation results.[34] NMR results from He and co-workers[20] with CEC = 58 mequiv/100 g, NMe_3-C_{16}, further show that less than quantitative cation exchange (0.2−0.5) increases the amount of anti conformations (peak at 33 ppm), even though IR frequencies edge up a few cm^{-1}.[20] This is evidence that hydrocarbon chains prefer a higher fraction of anti conformations when packing restraints are diminished (section 3.4).

At high CEC with NH_3 head groups, IR data for the series C_6 to C_{18} are available.[12] The clay mineral, fluorohectorite, is structurally similar to montmorillonite with a CEC of 150 mequiv/100 g.[12] A decrease in gauche conformations was observed by decreasing wavenumbers from 2932 cm^{-1} (C_6) to 2921 cm^{-1} (C_{18}) for the antisymmetric CH_2 stretching vibration. Reference frequencies for the neat alkylammonium salt in the liquid and in the crystalline state were determined as 2929 and 2918 cm^{-1}. These numbers suggest a higher fraction of gauche conformations than that in a liquid for C_6 and a remaining amount of gauche conformations for C_{18}. This trend is very closely the same in the simulation (Figure 4c), where 45% gauche is found in C_6 vs 39% in liquid C_{19}, and 25% gauche for longer chains on montmorillonite. The high percentage of gauche conformations for short chains agrees with the proposed hydrogen bonds between the NH_3 head group and the surface of the clay mineral (section 3) as well as earlier suggestions by Lagaly and Weiss.[8] Upon heating, an increase in wavenumbers (2921 → 2928 cm^{-1}) for C_{18} was observed[12] while only a minimal reversible peak in the DSC trace is found (section 4.3).[25] A significant reversible phase transition was not seen in the simulation, in agreement with DSC. Here it becomes apparent that IR spectroscopy is very sensitive to the detection of conformational changes that may not pertain to a reversible phase transition.

4.3. Thermal Behavior. The thermal properties of organically modified montmorillonites[12,19,21,22,25] have been analyzed with differential scanning calorimetry (DSC), in addition to X-ray diffraction, IR, and NMR spectroscopy.

A broad, diffuse peak is seen in all DSC traces on first heating.[12,19,21,22,25] This transition is not reversible and disappears on second heating. It is the annealing process described in section 4.1, in which the edge-on surfactants undergo a reorientation on the surface to minimize the energy and a few head groups move laterally on the surface to improve packing. The process is consistent with findings on self-assembled monolayers on other interfaces where head group arrangement and the degree of crystallinity of the chains determines the packing density.[26,53−55]

For low CEC (58, 72, and 90 mequiv/100 g), NMe_3 head groups, C_{16} and C_{18} chains, DSC shows no reversible phase transitions[19,21,22,25] in agreement with simulation.[34] This is associated with an overall liquid-like state, even though the degree of disorder varies with chain length (Figures 3c and 4c).

For high CEC (150 mequiv/100 g), NMe_3 and NH_3 head groups, and C_{18} chains, a small, essentially negligible reversible melting process was found.[12,25] Similar to lower CEC, it appears that a priori disordered alkyl chains cannot transition to higher disorder on heating, in agreement with simulation (Figure 4c).

5. Conclusions

The influence of cation exchange capacity (CEC), head group chemistry, and chain length on the self-assembly of alkyl chains on montmorillonite was analyzed using molec-

(51) Lacks, D. J. *Phys. Rev. Lett.* **2001**, *87*, 225502:1−4.
(52) Mirau, P. A. *A Practical Guide to Understanding the NMR of Polymers*; Wiley-VCH: Darmstadt, 2005.
(53) Bain, C. D.; Whitesides, G. M. *Science* **1988**, *240*, 62−63.
(54) Kessel, C. R.; Granick, S. *Langmuir* **1991**, *7*, 532−538.
(55) Tao, Y. T.; Wu, C. C.; Eu, J. Y.; Lin, W. L.; Wu, K. C.; Chen, C. H. *Langmuir* **1997**, *13*, 4018−4023.

ular dynamics simulation and experimental data. The emphasis is on typical systems with CECs of 91 and 145 mequiv/100 g, NH_3 and NMe_3 head groups, a series of hydrocarbon chains from C_2 to C_{22}, and on linking XRD, DSC, IR, and NMR data to information about molecular structure.

While both NMe_3 and NH_3 head groups are bonded ionically to the surface, NH_3 head groups can form three additional N−H···O−Si hydrogen bonds to the surface. Therefore, primary ammonium head groups are closely attached to the surface (H···O distance 150 pm), have a lower lateral mobility, and enforce extra gauche conformations in the backbones to maintain energetically favorable hydrogen bonds. NMe_3 head groups are larger in size, flexibly bonded to the surface (H···O distance 290 pm), and do not impose extra restraints on chain conformations. The absence of hydrogen bonds facilitates more frequent rearrangements across cavities in the surface. For example, small quaternary ions like Me_3NEt^+ move across the surface of a single montmorillonite layer (CEC = 91 mequiv/100 g) with a two-dimensional diffusion constant of 5.0×10^{-6} cm^2/s (∼20% the value for three-dimensional liquid water under ambient conditions).

The comparatively low surface saturation with alkyl chains in these systems leads to structures of alkyl multilayers with essentially parallel orientation to the surface. Monolayers, bilayers, and trilayers are successively formed in the order C_{10}, C_{22} (CEC = 91, NH_3 head group) and C_6, C_{12}, C_{18} (CEC = 145, NH_3 head group). NMe_3 head groups shift the onset of steps in basal plane spacing by ∼2 carbon atoms. The increase in basal plane spacing with increasing chain length occurs in well-defined steps at low CEC and in a more steady progression at high CEC. In this regard, simulation confirms prior conclusions.

Formation of successive hydrocarbon layers between the layered silicate layers with increasing chain length causes periodic fluctuations in interlayer density. Minima are found for partially formed layers, maxima are found for fully packed layers, and convergence to a homogeneous interlayer structure and density is seen for emerging 4-layers (∼C_{20} at CEC = 145). The interlayer density approaches a limit of 730 kg/m^3, compared to 790 kg/m^3 for crystalline surfactant, and the average fraction of gauche conformations is 27%.

While conformations of the hydrocarbon backbones would ideally be all-anti at room temperature (∼5% gauche in the crystalline state), we identified the factors that determine the higher percentage of gauche conformers in the surfactants. Primarily, the density of charge defects (CEC) enforces the arrangement of surfactants and determines a basic degree of conformational disorder, up to 20% gauche. Secondarily, the mode of head group binding, such as N−H···O−Si hydrogen bonds in $R-NH_3^+$ head groups versus flexible bonding of $R-N(CH_3)_3^+$ head groups, can increase the percentage of gauche conformations by up to 20%. Tertiary, also the amount of confinement between the silicate layers, as reflected by the interlayer density, can increase the percentage of gauche conformations by up to 20%. Overall, between 15% and 45% gauche conformations were found in the series of alkylammonium-modified montmorillonites (compare to 39% in liquid *n*-octadecylamine) due to a combination of these effects.

Formation of alkyl layers proceeds also weakly on the outer surface of montmorillonite, even though smaller changes in average conformation as a function of chain length are found.

The relationship between computational (molecular dynamics) and experimental data was found to be very complementary. Basal plane spacings from X-ray diffraction and from simulation agree within ±5%. The experimentally observed annealing process could be simulated and identified as a reorientation of the alkyl chains to improve packing. DSC, IR, and NMR measurements give qualitative insight into chain conformations, which agree with quantitative conformational data from the simulation. To the best of our knowledge, the size of the computational data set surpasses prior experimental work in the area and will provide guidance in the choice of alkyl modifiers for interactions with solvents, polymers, and other nanoscale buiding blocks.

Acknowledgment. We are grateful to the Air Force Office of Scientific Research, to the Air Force Research Laboratory (AFRL), Wright-Patterson Air Force Base, and to Wright State University, Dayton, Ohio, for support. Helpful discussions with Lawrence Drummy and Peter Mirau are acknowledged.

CM062019S